Manoeuvring of an aquatic soft robot using thrust-vectoring

Manoeuvring of an aquatic soft robot using thrust-vectoring

Tao Wang [1], Artur K. Lidtke[1,2], Francesco Giorgio-Serchi[3,*] and Gabriel D. Weymouth [1]

***Abstract*— Capability of a pulsed-jetting, aquatic soft robot to perform turning manoeuvres by means of a steerable nozzle is investigated experimentally for the first time. Actuation of this robot is based on the periodic conversion of slowly-charged elastic potential energy into fluid kinetic energy, giving rise to a cyclic pulsed-jet resembling the one observed in cephalopods. A steerable nozzle enables the fluid jet to be deflected away from the vehicle axis, thus providing the robot with the unique ability to manoeuvre using thrust-vectoring. This actuation scheme is shown to offer a high degree of control authority when starting from rest, yielding turning radii of the order of half of the body length of the vehicle. The most significant factor affecting efficiency of the turn has been identified to be the fluid momentum losses in the deflected nozzle. This leads, given the current nozzle design, to a distinct optimum nozzle angle of 35°.**

I. INTRODUCTION

The need for an increased degree of automation in underwater operations consistently require Autonomous Underwater Vehicles (AVU) and Remotely Operated Vehicles (ROV) to deal with often overwhelming challenges. These commonly encompass the complexity of navigation in unstructured submerged scenarios, the low-bandwidth communication between the vehicle and the surface and, most importantly, the hazardous nature of the sea climate where adverse weather conditions may prevent intervention altogether [1].

The inspiration from sea-dwelling organisms is sometimes regarded as a viable way to devise disruptive designs which offer the benefit of enhanced propulsive performance and improved manoeuvrability [2], [3], [4]. Because of this, bio-inspired aquatic robots have become widespread [5] and, among these, soft robots are starting to earn recognition [6].

Among the many sources of inspiration, cephalopods (i.e. squids and octopuses) stand out for their combination of utmost bodily softness and exceptional swimming capability. Cepahlopods are almost completely lacking a supportive skeletal structure and, as a consequence of this, they employ a propulsive routine which does not rely on the reciprocal motion of joints, contrary to the more prevalent use of flapping-based force generation mechanisms [7]. Quite the opposite, cephalopods' propulsion is based on the expulsion of finite jets of water which they execute by the periodic pulsation of a cavity of their body [8].

Nowadays, a broad body of literature exists which addresses the distinctive features of pulsed-jet propulsion. This brings evidence that large viscous [9], [10], [11], [12] and inertial [13], [14] fluid effects are concomitant in making cephalopod-inspired locomotion very effective both as a quasi-steady, sustained swimming mode as well as a short-range, highly menoeuvreable one, thanks, in part, to their structural flexibility [15], [16].

Consequently, several actutors capable of replicating this discontinuous, sometimes asymmetric, pulsating routine exist either as stand-alone systems [17], [11], [18], [12] or as part of fully self-propelled vehicles [19], [20], [21], [22]. However, while major efforts have been devoted to study the fluid dynamic effects associated with the pulsating routine and propulsive efficiency of such systems, very limited work has been focused on manoeuvrability of systems endowed with such a mode of propulsion [23], [24]. Addressing this niche is the main aim of the present study. To the best of the authors' knowelege, this work reports, for the first time, an experimental investigation on the maneuvrability of soft-bodied, pulsed-jet, underwater vehicles.

Specifically, an existing design of a soft fluidic actuator, used previously in a captive configuration for thrust measurements [25], was fitted with a steerable nozzle to allow thrust vectoring, as well as straight-ahead propulsion. The system was then installed in a laboratory-scale, soft-bodied, remotely operated vehicle. To estimate the manoeuvrability of the robot subject to different jet deflections, a series of tests were carried out where the trajectory of the vehicle was tracked using an overhead motion capture system.

The collected data provide preliminary insights into the benefit of using thrust-vectored, pulsed-jet propulsion as a singular means of designing soft unmanned underwater

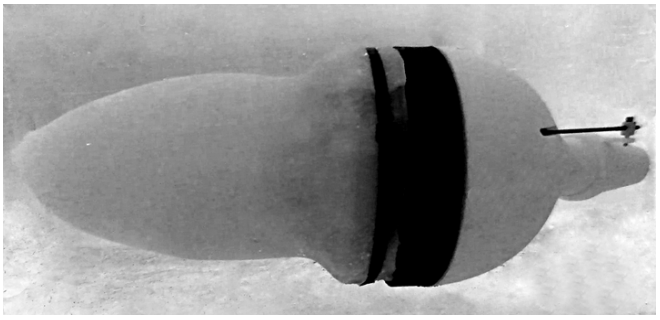

Fig. 1: Photograph of the robot in deflated configuration with the steerable nozzle at the back (robot facing left).

[1]Fluid Structure Interaction Group, University of Southampton, SO16 7QF Southampton, UK
[2]Maritime Research Institute Netherlands (MARIN), Haagsteeg 2, 6708 PM, Wageningen, The Netherlands
[3]Scottish Microelectronics Center, School of Engineering, University of Edinburgh, EH9 3FF Edinburgh, UK
[*]*Corresponding author's e-mail:* f.giorgio-serchi@ed.ac.uk

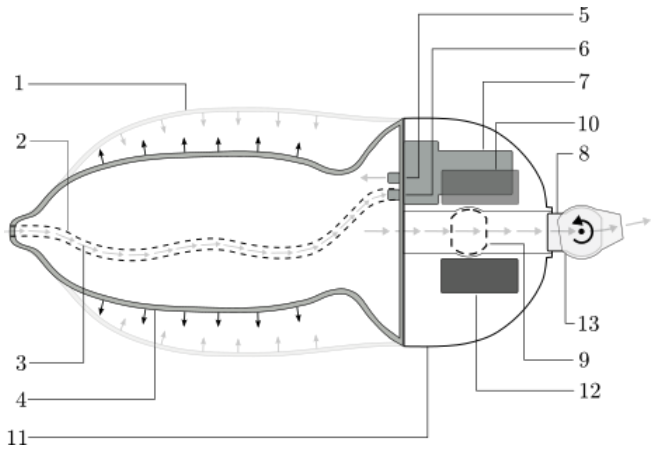

Fig. 2: (a) Schematic depiction of the robot components. (1) elastic membrane in the inflated state, (2) internal hose for fluid ingestion, (3) fluid flow during suction, (4) elastic membrane in the collapsed state, (5) pump exhaust, (6) pump inlet, (7) centrifugal pump, (8) steerable nozzle support, (9) ball valve, (10) servo motor for valve control, (11) rigid compartment, (12) servo for nozzle rotation control, (13) steerable nozzle.

vehicles with superior maneuvrability.

II. ROBOT DESIGN

A. General arrangement

The robot, shown in Fig. 1, consists of an elastic hollow membrane fitted onto a rigid stern segment, which contains the subsystems required for coordinating the inflation/deflation routine and the thrust-vectoring. These are: a pump, a valve, and a servo-actuated steerable nozzle. These are schematically depicted in Fig. 2. Length overall of the robot is 295 mm.

Control of the robot is carried out using a micro-controller unit (MCU), which executes actions in a pre-programmed manner controlled by the user. Currently, control signals from the MCU and power from a 12 V DC power supply are sent to the robot via an umbilical cable due to the small scale of the robot. However, because all of the mechanical subsystems have been successfully integrated into the robot, a larger, untethered variant could be readily built with the control logic and batteries fitted inside the robot.

B. Pulsed jet actuator

The actuation of the system entails a periodic sequence of slow expansion of the elastic cavity, followed by its abrupt collapse upon controlled opening of the valve. Inflation of the membrane is driven by the pump, which ingest ambient fluid from in front of the vehicle and injects it into the internal cavity, progressively expanding the elastic walls of the membrane. At this stage, unwanted leakage of the fluid from the cavity is prevented by the closure of the valve. Upon reaching the desired extent of expansion of the membrane, the valve is actuated open, enabling the sudden outflow of the fluid across the nozzle under the effect of the restoring force exerted by the strained membrane. Rotation of the nozzle allows the jet to be oriented, thus exerting a forward thrust and a yaw moment on the body of the vehicle, enabling it to execute turning manoeuvres.

A total of two actuators are used to propel the vehicle: a servo for operating the valve and a pump for inflating the cavity. The actuators are fitted in the rigid section of the robot, item (11) in Fig. 2. The solid stern is used to support the aft end of the flexible, hollow membrane. This is a 4 mm thick, 250 mm long axi-symmetric ellipsoid truncated at 75% of its length made from silicone rubber cast in a 3D-printed mould. The pump used for inflating the mantle is a centrifugal M510 series TCS-micropump, item (7) in Fig. 2, rated at a 8.7 L/min top flow rate and 586 mbar maximum head pressure. Rotational speed of the pump is controlled using an electronic speed controller (ESC). The flow release is regulated by a custom-printed ball-valve, item (9), actuated by a Traxxas 2080 waterproof servo, item (10) in Fig. 2. Detailed arrangement of these components is described in details in [25] and [26].

C. Steerable nozzle

The current version of the robot is appended with a steerable nozzle, Fig. 3(a), which enables thrust vectoring. This comprises of two 3D-printed components: a stationary nozzle support, item (8) in Fig. 2, and a moving external part, item (13), which constitutes the actual steerable nozzle. The latter is fitted onto the nozzle support via a pivot located at its centre of rotation. The angle of the thrust-vectoring part is adjusted using a servo identical to the one used for opening

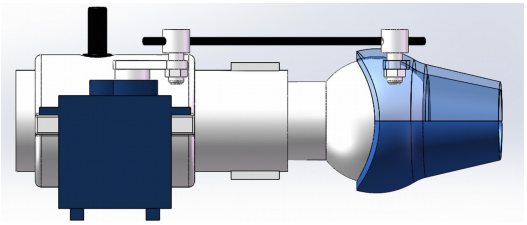

(a) Side view of the thrust-vectoring unit

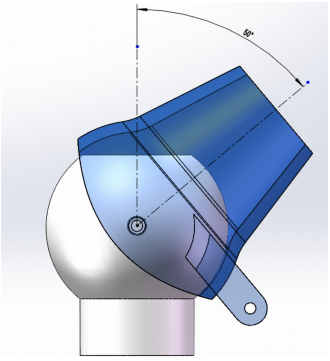

(b) Top view of the nozzle

Fig. 3: The steerable nozzle: (a) side view of the thrust-vectoring component. In the foreground, the servo motor, with the shaft linked by a crank to the steerable nozzle (in blue); (b) top view of the steerable nozzle at 50° deflection.

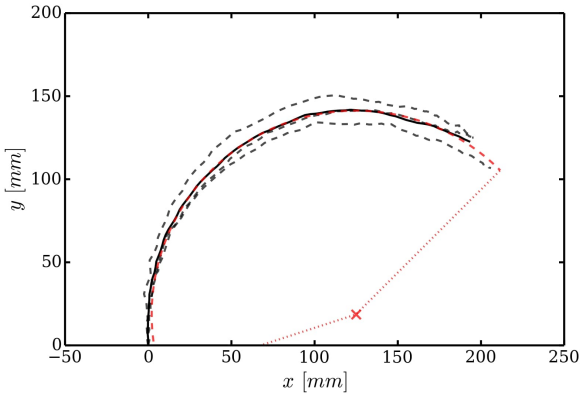

Fig. 4: Robot trajectory with a 25° nozzle deflection. Dashed black lines are the tracked trajectories from repeated tests, the continuous black line is a moving average of the three trajectories, and the dashed red line is the circle fitted to the mean data using least-squares method.

the nozzle valve. A crank links the shaft of the servo motor to a pin extruded sideways of the movable unit of the nozzle, Fig. 3(b). This enables the rotation of the shaft of the servo to control the deflection of the nozzle over a 100° span.

III. METHODOLOGY

A. Problem statement

In the present tests, focus is put on characterisation of the freely-moving system subject to the turning moment and forward thrust generated by pulsed-jet thrust-vectoring. The experiments are performed by recording the displacement of the robot subject to a single burst of speed when starting from rest. This forms a continuation of the previous work carried out with the same robot held in a captive configuration and used to study the effect of different fixed-shape nozzles on the developed forward thrust and static yaw moment [25].

B. Test matrix

To study the effect of variable nozzle angle, this was set to values between 5 and 50° at 5° increments. For each setting, three repeat measurements were carried out in order to provide an average response and give an indication of the degree of repeatability of these tests.

Each experimental run entailed an initial 15 s duty cycle of pump actuation, which inflated the elastic cavity to 0.9 litres, providing a 30% volume increase from the initial unstrained state of the mantle chamber. The nozzle was then deflected to the desired position and successively the main valve was opened for a period of 0.5 seconds, expelling a finite amount of fluid which propelled the robot forward from rest and induced a turning moment.

C. Experimental set up

The tests were performed in a 30.0x2.4x1.2 m tank, large enough for the robot to never come close to the boundaries of the testing facility during a single test run. Motion of the robot was tracked using a downward-facing camera held

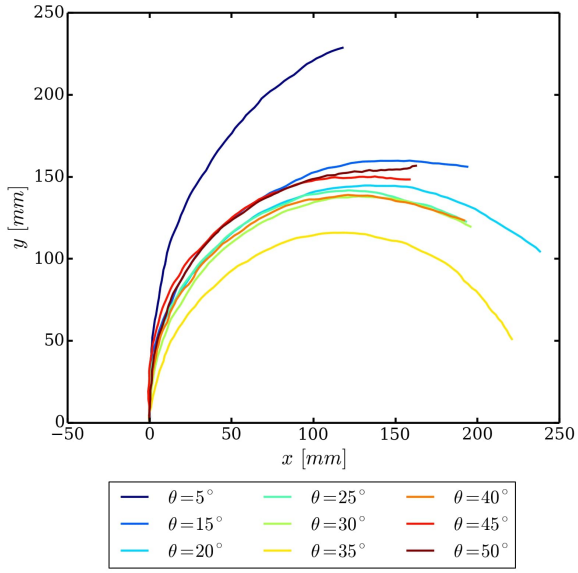

Fig. 5: Trajectories of the turning manoeuvre for nozzle deflections at 5, 15, 20, 25, 30, 35, 40, 45 and 50°.

stationary 2.0 m above the free surface. This guaranteed that the robot would never reach the boundaries of the recording area where image distortion could affect accuracy of trajectory tracking.

The experiments were initiated with the Centre of Mass (CoM) of the vehicle placed in the origin of an xy coordinate frame coincident with the centre of the recording frame and with the nozzle exit plane oriented in the negative y direction. Each run was recorded with the vehicle initially at rest and lasted until the robot had come to a complete stop.

D. Data analysis

An example of the resultant trajectory obtained for three successive repetitions of the same test is shown in Fig. 4 for

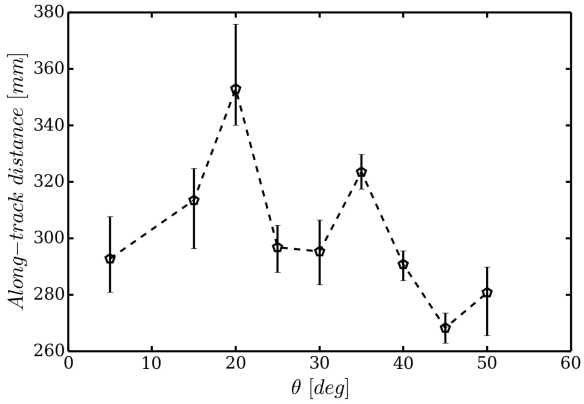

Fig. 6: Along-track distance travelled by the robot during the experiments as a function of the nozzle angle. Markers indicate mean values for each nozzle angle and error bars denote the minimum and maximum value measured for each condition.

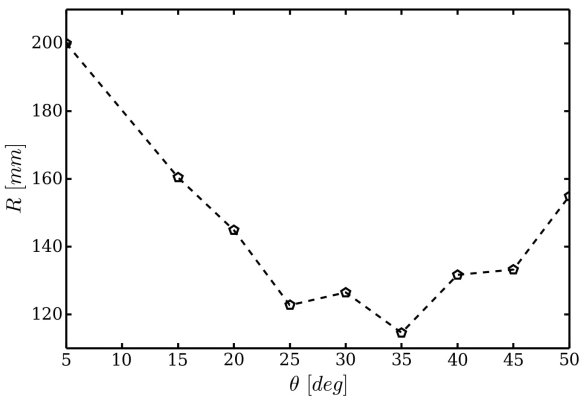

Fig. 7: Turning radii estimated for the vehicle as a function of the nozzle angle.

nozzle deflection of 25°. The test manifest a good degree of reproducibility with similar paths travelled by the robot, as well as comparable final position and orientation. For the remainder of the analysis, mean trajectories resulting from averaging the three repetitions are used.

Due to the motion of the robot being transient and dynamic by nature, it could not reach a steady turn. Thus, traditional methods used to analyse tactical diameter manoeuvres of ships [27] could not be readily applied to the problem at hand. However, from tracking the motion of the vehicle during a complete manoeuvre, its pose (heading) and tangential velocity could be extracted. These may be viewed as critical parameters defining the efficacy of the jet propulsor to induce rotation and forward acceleration. From a biological perspective, these would indicate the ability of the agent to initiate a rapid manoeuvre either to catch prey or avoid an imminent predator attack.

Furthermore, arcs could be fitted to the measured trajectories using least-squares method, with the tunable parameters being the centre or rotation and its diameter. In the light of lack of steady turn information, this data provided an estimate of the turning rate of the vehicle, as well as its turning radius, both of which can be readily compared against classical marine vehicles, bearing in mind the specifics of the method of locomotion of the present robot. An illustration of the result of this procedure is also depicted in Fig. 4.

IV. RESULTS

Fig. 5 presents mean trajectories of the vehicle as measured throughout the test campaign. Compared to the overall length of the robot of 295 mm, the observed paths travelled indicate that the vehicle is capable of travelling the order of one body length per a single release of the fluid jet. This is evident from examining the along-track distance computed from the data and shown in Fig. 6.

By fitting an equation of an arc to each trajectory using a least-squares method, average turning radius of the vehicle during the single manoeuvre could be computed. This is depicted in Fig. 7 for all test cases. All of the measured values vary between 70% and half of the body length of the

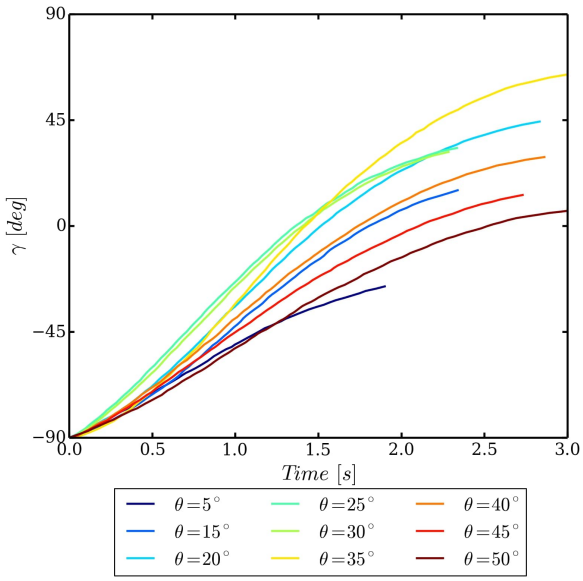

Fig. 8: Temporal profile of the robot heading during the turning manoeuvre for nozzle deflections at 5, 15, 20, 25, 30, 35, 40, 45 and 50°.

vehicle. A clear minimum is also observed around the nozzle angle of 35°, indicating the tightest turn.

The latter trend is consistent with the measured change in vehicle heading, shown in Fig. 8 as a function of time and nozzle angle. The best result from this perspective was also achieved with the nozzle deflected to 35°. In this case, during a single pulsation of 0.5 sec the robot was able to turn by approximately 160°, all the while starting from rest.

Collected data also allows for analysis of time-resolved velocity profiles, shown in Fig. 9 and 10 for the along-track and radial components, respectively. The shape of both curves reveals that both velocities increase rapidly over the first 1 s following the opening of the valve and release of the jet of the fluid; the robot may then be seen to slowly decelerate. For the axial velocity, a trend is observed whereby the higher the angle of the jet, the lower the maximum forward speed, albeit this starts to occur only for jet angles in excess of 20 degrees. This may be explained by part of the jet energy being utilised to induce the yaw moment rather than provide an axial force component. An exception to this observation is the data measured for a 5° displacement that appears to be an outlier in this respect. It is expected that this would have been caused by the robot being affected by the pull of the tether more significantly in this case because of moving much further from the origin than in the other test cases. In case of the radial velocity, the most apparent trend is the non-linear variation of the maximum turning rate. This may be seen to first increases with the nozzle angle but then deteriorate past 35° of deflection.

V. DISCUSSION

The presented data have revealed that the optimum angle of the nozzle for the robot is 35°. This has yielded the high-

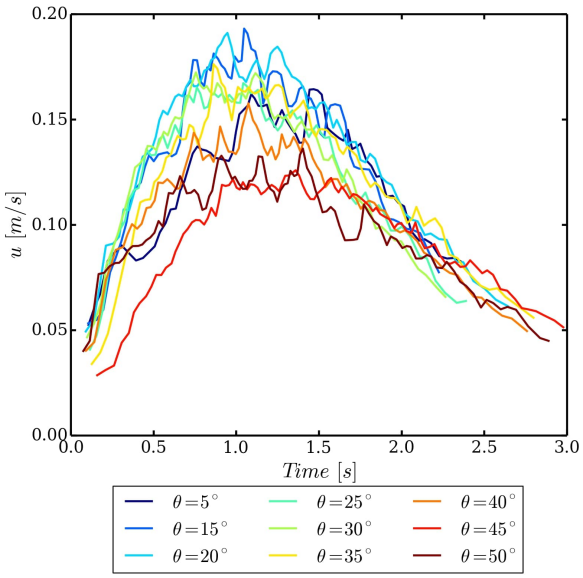

Fig. 9: Temporal profile of tangential velocity during the turning manoeuvre for different nozzle deflections.

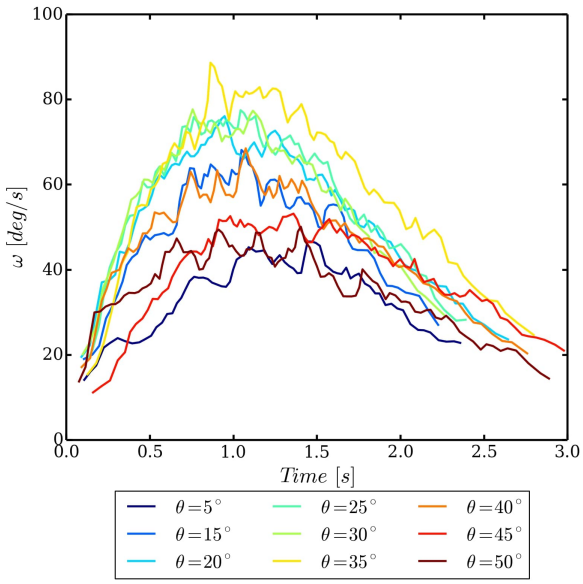

Fig. 10: Temporal profile of angular velocity during the turning manoeuvre for thte investigated nozzle deflections.

est turning rate, smallest turning radius, and larger overall change in the heading during the examined turn manoeuvres. Loss of performance beyond this operating point may be attributed to the loss of thrust induced by flow occlusion and significant viscous losses due to the appearance of sharp corners within the nozzle conduit. This loss of usable thrust has an impact on the associated yaw moment which, in turn, yields a visible decrease in turning moment, rate of rotation and an increase in the overall turning radius. This presents a limit to the operating range of the current design as, in theory, a nozzle could potentially be used to turn the vehicle in place should it be deflected by 90° to the vehicle axis. However, achieving such large angles presents severe practical difficulties if acceptably low losses are to be achieved.

The measured rapid acceleration of the robot, both in terms of axial and radial velocities, stands in agreement with the previously reported force measurements [25]. Those revealed the thrust generated by the jet to be impulsive in nature and reach the maximum value approximately 0.2 s after the jet is produced, or approximately 0.8 s before the maximum velocities were observed in the current self-propelled tests.

The most major obstacle in analysing the current data stems from the peculiar nature of the tested vehicle. Due to the impulsive nature of its propulsion system, the rapid change of its mass as the fluid jet is released, as well as change of the added mass due to the severe shape variation, attained velocities were measured to experience a high degree of variability throughout the turn manoeuvre. Furthermore, as steady turns could not be achieved, classical manoeuvrability analysis techniques, such as tactical diameter turn or a zig-zag manoeuvre, could not be readily used. Instead, the most representative mean and otherwise indicative quantities had to be extracted from the data. While informative, these do not entirely capture the behaviour of the robot, which indicates that further work is needed to achieve a more meaningful comparison to conventional marine vehicles.

VI. CONCLUSIONS

The present investigation has revealed that a pulsed-jet propulsor with a thrust-vectoring mechanism can be successfully used to manoeuvre an underwater vehicle without using additional control surfaces or hydrodynamic actuators. Current tests were performed with the robot starting from rest, demonstrating impressive capability to turn at very low initial speed. However, continued work is needed to further understand the hydrodynamic mechanisms affecting manoeuvring performance of this category of marine vehicles at finite speed. Most importantly, an accurate study of the manoeuvrability of mass-varying systems needs to be undertaken in order to accurately characterize the dynamics of this class of vehicles [28], [29]. Indeed, the variation of mass and added-mass [30] of this vehicle during a turning manoeuver significantly affects the turning moment and prevents the traditional dynamics equation employed for other thrust-vectoring systems to be employed here. From a design perspective, the most significant improvement needed is achievement of higher and more uniform forward speeds and construction of a variant of the robot independent of the shore-based power source and control logic.

Comparing the data for different nozzle angles indicates that for intermediate settings of approximately 20° remarkable turning performance may be achieved without sacrificing forward speed. Importantly, the proposed design has displayed an outstanding ability to perform turns with a radius of the order of half the body length and change its course by up to 45° while starting from rest. This is a close

match with some of the best performing aquatic organisms [31], [32]. The aforementioned trends put the current design in a unique relation with respect to classical propeller-driven vehicles and fish-inspired robots, which either require a finite forward speed or the execution of a complex kinematics mediated by multiple actuators to achieve a similar level of manoeuvrability [4].

REFERENCES

[1] I. Vasilescu, C. Detweiler, M. Doniec, D. Gurdan, S. Sosnowski, J. Stumpf, and D. Rus, "Amour v: A hovering energy efficient underwater robot capable of dynamic payloads," *The International Journal of Robotics Research*, vol. 29, pp. 547–570, 2010.

[2] J. Yu, R. Ding, Q. Yang, M. Tan, W. Wang, and J. Zhang, "On a bio-inspired amphibious robot capable of multimodal motion," *IEEE Transactions on Mechatronics*, vol. PP, pp. 1–10, 2011.

[3] F. Liu, K. M. Lee, and C. J. Yang, "Hydrodynamics of an undulating fin for a wave-like locomotion system design," *IEEE Transactions on Mechatronics*, vol. PP, pp. 1–9, 2011.

[4] J. Yu, C. Zhang, and L. Liu, "Design and control of a single-motor-actuated robotic fish capable of fast swimming and maneuverability," *IEEE/ASME Transactions on Mechatronics*, vol. 21, no. 3, pp. 1711–1719, June 2016.

[5] P. R. Bandyopadhyay, "Trends in biorobotic autonomous undersea vehicles," *IEEE Journal of Oceanic Engineering*, vol. 30, pp. 109–139, 2005.

[6] M. Calisti, G. Picardi, and C. Laschi, "Fundamentals of soft robot locomotion," *Journal of The Royal Society Interface*, vol. 14, no. 130, 2017. [Online]. Available: http://rsif.royalsocietypublishing.org/content/14/130/20170101

[7] M. Sfakiotakis and D. P. Tsakiris, "Biomimetic centering for undulatory robots," *The International Journal of Robotics Research*, vol. 26, pp. 1267–1282, 2007.

[8] W. Johnson, P. D. Soden, and E. R. Trueman, "A study in met propulsion: an analysis of the motion of the squid, *Loligo Vulgaris*," *Journal of Experimental Biology*, vol. 56, pp. 155–165, 1972.

[9] M. Gharib, E. Rambod, and K. Shariff, "A universal time scale for vortex ring formation," *Journal of Fluid Mechanics*, vol. 360, pp. 121–140, 1998.

[10] P. S. Krueger and M. Gharib, "The significance of vortex ring formation to the impulse and thrust of starting jet," *Physics of Fluid*, vol. 15, pp. 1271–1281, 2003.

[11] J. O. Dabiri and M. Gharib, "A revised slug model boundary layer correction for starting vorticity flux," *Theoretical and Computational Fluid Dynamics*, vol. 17, pp. 293–295, 2004.

[12] M. Krieg and K. Mohseni, "Modelling circulation, impulse and kinetic energy of starting jets with non-zero radial velocity," *Journal of Fluid Mechanics*, vol. 79, pp. 488–526, 2013.

[13] G. Weymouth and M. Triantafyllou, "Ultra-fast escape of a deformable jet-propelled body," *Journal of Fluid Mechanics*, vol. 721, pp. 367–385, 2013.

[14] F. Giorgio-Serchi and G. D. Weymouth, "Can added-mass variation act as a thrust force?" in *IEEE/MTS Oceans*, Aberdeen, UK, June 2017.

[15] ——, "Underwater soft robotics, the benefit of body-shape variations in aquatic propulsion," in *Soft Robotics: Trends, Applications and Challanges*, ser. Biosystems & Biorobotics. Springer, 2016, vol. 17, pp. 37–46.

[16] F. Corucci, N. Cheney, F. Giorgio-Serchi, J. Bongard, and C. Laschi, "Evolving soft locomotion in aquatic and terrestrial environments: Effects of material properties and environmental transitions," *Soft Robotics*, vol. 5, no. 4, pp. 475–495, 2018. [Online]. Available: https://doi.org/10.1089/soro.2017.0055

[17] P. S. Krueger, "Measurement of propulsive power and evaluation of propulsive performance from the wake of a self-propelled vehicle," *Bioinspiration and Biomimetics*, vol. 1, pp. 49–56, 2006.

[18] L. A. Ruiz, R. W. Whittlesey, and J. O. Dabiri, "Vortex-enhanced propulsion," *Journal of Fluid Mechanics*, vol. 668, pp. 5–32, 2011.

[19] A. A. Moslemi and P. S. Krueger, "Propulsive efficiency of a biomorphic pulsed-jet underwater vehicle," *Bioinspiration and Biomimetics*, vol. 5, pp. 1–14, 2010.

[20] M. Krieg and K. Mohseni, "Dynamic modeling and control of biologically inspired vortex ring thrusters for underwater robot locomotion," *IEEE Transactions on Robotics*, vol. 26, pp. 542–554, june 2010.

[21] F. Giorgio-Serchi, A. Arienti, and C. Laschi, "A soft unamnned underwater vehicle with augmented thrust capability," in *MTS-IEEE OCEANS*, San Diego, CA, USA, September 2013.

[22] F. Giorgio-Serchi, A. Arienti, F. Corucci, M. Giorelli, and C. Laschi, "Hybrid parameter identification of a multi-modal undwater soft robot," *Bioinspiration & Biomimetics*, vol. 12, no. 2, p. 025007, 2017.

[23] F. Renda, F. Giorgio-Serchi, F. Boyer, and C. Laschi, "Structural dynamics of a pulsed-jet propulsion system for underwater soft robots," *International Journal of Advanced Robotic Systems*, vol. 12, no. 6, p. 68, 2015. [Online]. Available: https://doi.org/10.5772/60143

[24] F. Renda, F. Giorgio-Serchi, F. Boyer, C. Laschi, J. Dias, and L. Seneviratne, "A unified multi-soft-body dynamic model for underwater soft robots," *The International Journal of Robotics Research*, vol. 0, no. 0, p. 0278364918769992, 0. [Online]. Available: https://doi.org/10.1177/0278364918769992

[25] F. Giorgio-Serchi, A. Lidtke, and G. Weymouth, "A soft aquatic actuator for unsteady peack power amplification," *IEEE/ASME Transactions on Mechatronics*, 2018.

[26] A. Lidtke, F. Giorgio-Serchi, and G. D. Weymouth, "A low-cost experimental rig for multi-dof unsteady thrust measurements of aquatic bioinspired soft robots," in *IEEE RAS RoboSoft*, Livorno, Italy, April 2018.

[27] T. I. Fossen, *Handbook of Marine Craft Hydrodynamics and Motion Control*. John Wiley & Sons, Ltd, 2011.

[28] A. Nanjangud and F. Eke, "On the Angular Momentum of Rockets, Balloons, and Other Variable Mass Systems," *arXiv e-prints*, p. arXiv:1612.00884, Dec. 2016.

[29] J. Hurtado, "Analytical dynamics of variable-mass systems," *Journal of Guidance, Control, and Dynamics*, vol. 41, no. 3, pp. 701–709, 2018.

[30] G. Weymouth and F. Giorgio-Serchi, "Analytic modeling of a size-changing swimmer," in *IUTAM Symposium on Critical flow dynamics involving moving/deformable structures with design applications*, Santorini, Greece, June 2018.

[31] E. D. Tytell and G. V. Lauder, "The c-start escape response of polypterus senegalus: bilateral muscle activity and variation during stage 1 and 2," *Journal of Experimental Biology*, vol. 205, no. 17, pp. 2591–2603, 2002. [Online]. Available: http://jeb.biologists.org/content/205/17/2591

[32] W. C. Witt, L. Wen, and G. V. Lauder, "Hydrodynamics of c-start escape responses of fish as studied with simple physical models," *Integrative and Comparative Biology*, vol. 55, no. 4, pp. 728–739, 2015.